DYNAMIC ANALYSIS OF A BEAM UNDER MOVING LOADS – VÁRZEAS BRIDGE CASE STUDY

Ruben Ribeiro
ruben.ribeiro@ist.utl.pt
Instituto Superior Técnico, Universidade de Lisboa, Portugal
November 2018

ABSTRACT

As the overall traffic increased in urbanized areas, so did the number of roads, bridges and routes in general. This increase in the number of bridges led to a larger number of bridge collapses. Over time, degradation of bridge components through fatigue (the main cause of failures of metallic structures) will take place, and undetected defects increase the rate at which the bridge degrades. This degradation needs to be estimated regularly and accurately using sophisticated monitoring systems. Ideally, computational models would be able to compute the impact of a vehicle crossing the bridge. Therefore, the aim of this thesis is to develop a model that accurately predicts the dynamic behavior caused on a bridge, with certain properties and geometries, by a vehicle with certain parameters. This model is then tested and applied to a case study (the Várzeas bridge structure), by computing the signals (or cycles) produced on this structure and comparing these signals with real signals measured by sensors. When this comparison is performed, the computational signals are very different from the real signals. However, by fitting the computational signals to the corresponding real signals, the optimized physical parameters (properties and geometries) for the model are obtained. On the one hand, the model appears to be valid, seeing that the accuracy of the computational signals can be controlled by fitting the bending stiffness of the structure, but on the other hand controlling the accuracy is very difficult without a significant amount of traffic data. Finally, this paper provides a computational procedure, which needs to include an optimization procedure of the physical parameters in future work.

Keywords: bridge structures, Euler-Bernoulli beam, dynamic model, MATLAB, computational model, fatigue, vehicle traffic, maintenance.

1. INTRODUCTION

Every year, a large number of bridges experience failure around the world [4]. The most recent major collapse occurred on August 14th, 2018, in Genoa (Italy), whose collapse caused at least 43 fatalities. According to the preliminary report of the collapsed Morandi bridge, this structure experienced failure due to a combination of factors, namely poor design, questionable building practices and insufficient maintenance [13].

Another famous bridge collapse also occurred in the current year (March 15th, 2018), in Florida (United States). This collapse resulted in 6 fatalities and 9 major injuries. In the preliminary report of the pedestrian bridge, it is mentioned that it collapsed during re-tensioning of the diagonal members on its north and south ends, as part of the design plans [2]. The bridge failed due to the initiation and propagation of a crack in the diagonal member of the north end. Whether this crack initiated because of the bridge design, construction process or materials used is still unclear.

At least 90% of all failures of metallic structures, including bridges, aircrafts and machine components, are caused by fatigue [10]. This percentage can be reduced by increasing the infrastructure budget, not only to increase the quality and quantity of inspections, but also to fix every defect detected by these inspections, no matter how small it seems. If this is unfeasible, or even impossible, other solutions to this problem must be thought and implemented, thereby reducing the significant amount of lives lost due to bridge collapses.

1.1 Objectives

The objective of this paper is the development of a dynamic analysis of a beam under moving loads to support a monitoring system for a given bridge structure, with the aim to predict the acceleration and strain cycles when a vehicle passes over it. This computational model is then applied to a case study of a bridge structure in Várzeas, by computing the signals (or cycles) produced on this structure and comparing these signals with real signals measured by sensors.

1.2 Document Structure

Including the introduction, this document is divided into six sections. Section 2 introduces the Euler-Bernoulli beam and the simply supported plate, which consist of structures that can be used as an approximation for more complex structures, for example bridges. The main objective of section 3 is to develop a computational model that returns the deformed shape of the bridge along time, caused by a passing vehicle, which is simulated by a set of moving loads. Section 4 analyzes the bridge structure of a case study, being that this structure is then used to estimate the acceleration and deformation signals computationally. In section 5, the results obtained by conducting several tests are explored and discussed using the computational model. Finally, section 6 presents the main conclusions withdrawn from the paper, as well as its limitations and respective improvements that can be implemented with future work.

2. LITERATURE REVIEW

Araújo and Silvestre (2014) affirmed that the transversal shear deformations can be neglected for thin plates and beams. In practice, this means that the cross-sections normal to a beam's axis before deformation remain plane and normal to the axis after deformation.

Reddy (1994) described the Euler-Bernoulli beam model extensively, which neglects the effects of transverse shear deformation. While this model is appropriate for thin beams, it is not appropriate for beams with a large thickness. Reddy also provided the stiffness matrix and force vector for an Euler-Bernoulli beam element, which are obtained using its governing equations, as well as the assembly method used to obtain the displacements of every node, when this beam is subjected to static loads.

Do et al. (2017) provided the dynamic component of the differential governing equation of the Euler-Bernoulli beam. This time-dependent term is used to obtain the mass matrix of an Euler-Bernoulli beam element.

Finally, Lee et al. (2017) provided the equation of motion which governs the vertical vibration of thin plates. This governing equation allows to calculate the natural frequencies of a thin plate with certain boundary and initial conditions.

3. COMPUTATIONAL MODEL

The acceleration and deformation signals produced by a vehicle can be estimated computationally. In its turn, the physical quantities required to estimate these signals (accelerations and displacements) are calculated for each instant of time using the finite element method. Observing that the equations of motion are solved using a numerical method, in which time is not treated as a continuous variable, but rather as a discrete variable, the points in time between the initial and final instants are separated from each other by a time step, or increment. This initial time instant corresponds to the moment when the front axle of a vehicle comes in contact with the bridge. Assuming a constant velocity v, every axle of a vehicle moves with the following distance increment:

$$\Delta x = v \cdot \Delta t \tag{1}$$

where Δt is the time increment, and v is the vehicle's velocity.

Each axle supports a certain percentage of the vehicle's weight and exercises a certain force on the bridge, as described by the following equation:

$$f_0 = m \cdot g \tag{2}$$

where g is the gravitational acceleration, and m and f_0 are the weight that is supported and force that is exercised on the bridge by a specific axle, respectively.

An axle's position can be defined by global or local coordinates. While the global coordinates are

relative to the beam, the local coordinates are relative to a specific element. To use finite elements, the force applied on an element needs to be converted into a vector of equivalent loads applied on the degrees of freedom of the respective element. This vector of nodal loads is obtained with the following equation:

$$\begin{Bmatrix} f_L \\ M_L \\ f_R \\ M_R \end{Bmatrix} = \{N\} \cdot f_0 \tag{3}$$

where $\{N\}$ represents the shape functions.

The shape functions are defined as follows:

$$\{N\} = \begin{Bmatrix} N_1 \\ N_2 \\ N_3 \\ N_4 \end{Bmatrix} \tag{4}$$

$$N_1 = 1 - 3\left(\frac{x}{l}\right)^2 + 2\left(\frac{x}{l}\right)^3 \tag{5}$$

$$N_2 = x\left(\frac{x}{l} - 1\right)^2 \tag{6}$$

$$N_3 = 3\left(\frac{x}{l}\right)^2 - 2\left(\frac{x}{l}\right)^3 \tag{7}$$

$$N_4 = x\left(\left(\frac{x}{l}\right)^2 - \frac{x}{l}\right) \tag{8}$$

where l is the length of an element, and x represents the local coordinates of an axle.

Once the nodal loads for each element and instant have been determined, the global load vector can also be assembled for each instant. Likewise, the global stiffness and mass matrices are calculated by assembling every elemental stiffness and mass matrix, respectively.

After that, the global stiffness and mass matrices are used to obtain the global damping matrix, with the Rayleigh damping theory [12]. Finally, the deformed shape of the bridge along time, which depends on the displacements, velocities and accelerations, is determined using Newmark's method [7]. This method requires the global load vector and the global stiffness, mass and damping matrices. When the deformed shape of the bridge along time is determined, the accelerations and deformations at half span are used to estimate the signals.

3.1 Rayleigh Damping Theory

Rayleigh damping is included in the viscous damping model and is defined as follows:

$$[C] = [M]\sum_{k=0}^{p-1} \alpha_k([M]^{-1}[K])^k \tag{9}$$

where p is the number of terms with a non-negative indexed coefficient.

This is a reasonable approximation for a reduced damping. By applying an orthogonal transformation to (3.9), the following equation is obtained:

$$[\varphi^T][C][\varphi] = \sum_{k=0}^{p-1} \alpha_k \omega_n^{2k-1} \tag{10}$$

where ω_n and ξ_n represent the bridge's natural frequencies and their corresponding damping ratios, and the columns of $[\varphi]$ are normalized mode shapes of the system.

The simplest Rayleigh damping is obtained when $p = 2$. This damping matrix is proportional to both the stiffness and mass matrices.

$$[C] = \alpha_0[M] + \alpha_1[K] \tag{11}$$

$$2\xi_n = \alpha_0\omega_n^{-1} + \alpha_1\omega_n \tag{12}$$

To determine the coefficients α_0 and α_1, at least two values for the natural frequency, as well as their corresponding damping ratios, are needed.

3.2 Newmark Method

The Newmark method is a direct integration method that uses the following assumptions:

$$\{\dot{x}_{nc}\}_{t+\Delta t} = \{\dot{x}_{nc}\}_t + [(1-\delta)\{\ddot{x}_{nc}\}_t + \delta\{\ddot{x}_{nc}\}_{t+\Delta t}] \cdot \Delta t \tag{13}$$

$$\{x_{nc}\}_{t+\Delta t} = \{x_{nc}\}_t + \{\dot{x}_{nc}\}_t \cdot \Delta t + \left[\left(\frac{1}{2} - \alpha\right)\{\ddot{x}_{nc}\}_t + \alpha\{\ddot{x}_{nc}\}_{t+\Delta t}\right] \cdot \Delta t^2 \tag{14}$$

where α and δ are the parameters that influence the accuracy and stability of the integration, $\{x_{nc}\}$ are the linear and angular displacements of the non-constrained nodes, $\dot{()}$ represents a derivative with respect to time, and Δt is the time increment.

Solving from (3.14) for $\{\ddot{x}_{nc}\}_{t+\Delta t}$, the following equation is obtained:

$$\{\ddot{x}_{nc}\}_{t+\Delta t} = \frac{1}{\alpha \Delta t^2}(\{x_{nc}\}_{t+\Delta t} - \{x_{nc}\}_t) - \frac{1}{\alpha \Delta t}\{\dot{x}_{nc}\}_t - \left(\frac{1}{2\alpha} - 1\right)\{\ddot{x}_{nc}\}_t \quad (15)$$

The only variable left to determine to solve the system at time $t + \Delta t$ is $\{x_{nc}\}_{t+\Delta t}$. To do that, $\{\ddot{x}_{nc}\}_{t+\Delta t}$ from (3.15) and $\{\dot{x}_{nc}\}_{t+\Delta t}$ from (3.13) need to be substituted into the equations of motion at time $t + \Delta t$:

$$[M_{nc}]\{\ddot{x}_{nc}\}_{t+\Delta t} + [C_{nc}]\{\dot{x}_{nc}\}_{t+\Delta t} + [K_{nc}]\{x_{nc}\}_{t+\Delta t} = \{f_{nc}\}_{t+\Delta t} \quad (16)$$

$$\left[\widehat{K}\right]\{x_{nc}\}_{t+\Delta t} = \left\{\widehat{f_{nc}}\right\}_{t+\Delta t} \leftrightarrow \{x_{nc}\}_{t+\Delta t} = \left[\widehat{K}\right]^{-1}\left\{\widehat{f_{nc}}\right\}_{t+\Delta t} \quad (17)$$

where $[K_{nc}]$, $[M_{nc}]$ and $[C_{nc}]$ are the resultant stiffness, mass and damping matrices, respectively, after eliminating the rows and columns corresponding to the constrained degrees of freedom, and $\{f_{nc}\}$ is the resultant load vector after eliminating the rows corresponding to the constrained degrees of freedom.

The parameters $\left[\widehat{K}\right]$ and $\left\{\widehat{f_{nc}}\right\}_{t+\Delta t}$ can be solved by treating $\{\ddot{x}_{nc}\}_{t+\Delta t}$ and $\{\dot{x}_{nc}\}_{t+\Delta t}$ as functions of $\{x_{nc}\}_{t+\Delta t}$, $\{x_{nc}\}_t$, $\{\dot{x}_{nc}\}_t$ and $\{\ddot{x}_{nc}\}_t$. Now that the system is solved, the following algorithm can be applied: i) start the procedure with $t = 0$, ii) determine $\left\{\widehat{f_{nc}}\right\}_{t+\Delta t}$, iii) calculate the displacements at time $t + \Delta t$ with (17), iv) obtain the accelerations and velocities at time $t + \Delta t$ using (15) and (13), respectively, v) repeat until $t = t_{max}$.

4. CASE STUDY

The bridge structure explored in the present case study is located near Luso (Figure 1).

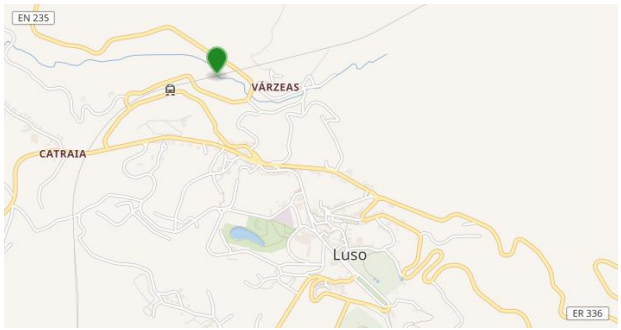

Figure 1: Case study bridge location (Luso). [1]

This bridge's main components are the longitudinal and cross girders, profiled sheet, reinforcements, concrete slab and bituminous pavement. Some of these components are shown in Figure 2.

Figure 2: Profiled sheet, longitudinal and cross girders.

Information about the main components from the descriptive memory [3] is presented in Tables 1 and 2, and its properties are presented in Tables 3 and 4.

Table 1: Information about the main components (1).

Component	Quantity (N)	$A\ [m^2]$	$h\ [mm]$
Cross girder	20	—	—
Longitudinal girder	4	0.038	—
Profiled sheet	—	213	1.2
Reinforcements	—	—	—
Slab + pavement	—	—	—

Table 2: Information about the main components (2).

$L\ [m]$	$V\ [m^3]$	$m\ [kg]$
2.35	—	134
19	—	—
—	—	—
—	—	8800
19	42	—

Table 3: Information about the main components (1).

Component	Material
Cross girder	IPE 360 steel
Longitudinal girder	S355 steel
Profiled sheet	S320GD steel
Reinforcements	S500 steel
Concrete (slab + pavement)	C30/37 concrete

Table 4: Information about the main components (2).

Density (ρ) [kg/m^3]	Poisson's ratio (υ)
7850	0.3
7850	0.3
7850	0.3
7850	0.3
2400	0.15

4.1 Sensors

Several accelerometers and extensometers, as well as other sensors that measure weather related values, namely relative humidity, precipitation, temperature and wind speed, have been strategically placed on the bridge under study, as can be observed in Figure 3 and Figure 4.

Figure 3: Visible extensometers (strain gauges).

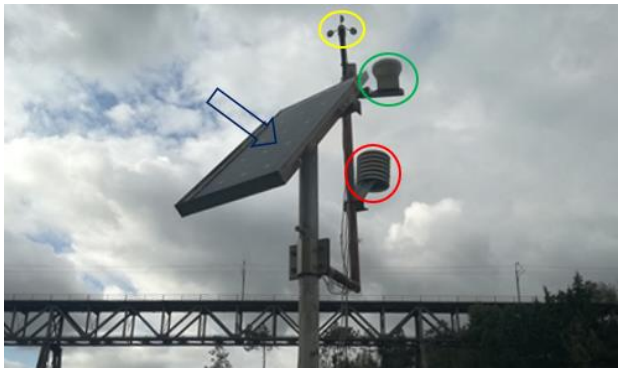

Figure 4: Weather sensors.

The weather sensors are activated periodically, but the accelerometers and extensometers are only triggered when a vehicle starts crossing the bridge. When triggered, these last sensors collect data for 5 seconds, or signals, with a frequency of 50 Hz. Both the acceleration and the deformation signals depend on the number of axles, weight and velocity of the passing vehicle, as well as on the weather conditions. While the vehicle parameters affect their amplitude, the weather conditions affect their mean value. Typical acceleration and deformation signals measured by the movement sensors are shown in Figure 5 and Figure 6, respectively.

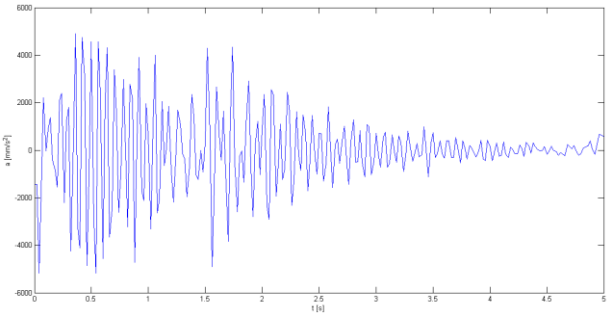

Figure 5: Typical acceleration signal.

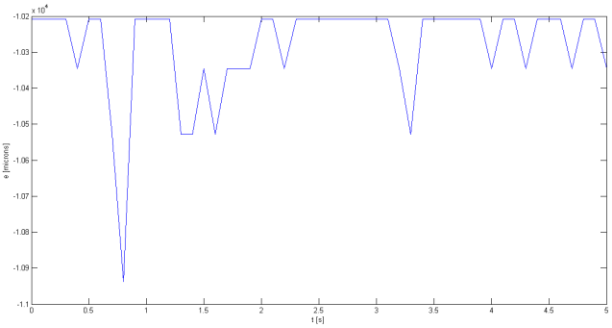

Figure 6: Typical deformation signal.

4.2 Simplified Bridge Model

A beam is defined by its density (ρ), Young's modulus (E), length (L), cross-sectional area (A) and second moment of inertia (I). Considering that a vehicle only causes appreciable deformation along its width, and that the width of an average vehicle is approximately two meters, the beam's width is also defined as $b = 2\,m$. Using this value, as well as the information presented in Table 1 and Table 2, the beam's properties and geometries are as follows:

- $\boldsymbol{\rho = \frac{m}{V} = 2940\ kg/m^3}$
- $\boldsymbol{A = \frac{b}{B} \cdot \frac{V}{L} = 0.5451\ m^2}$
- $h = \frac{A}{b} = 0.2726\ m$
- $\boldsymbol{I = \frac{1}{12} \cdot b \cdot h^3 = 3.38 \cdot 10^{-3}\ m^4}$

where m and V are the bridge's mass and volume, respectively, when only the main components are considered, $B = 9\,m$ and $L = 19\,m$ are the bridge's width and length, respectively, and h represents its equivalent thickness.

The only property left to determine is Young's modulus. Since the natural frequency of a structure is proportional to its vibration constant, being that the respective slope depends on Young's modulus, this property can be obtained by plotting a natural frequency versus plate vibration constant graph, using the vibration data collected from the bridge presented in Table 5.

Table 5: Bridge's vibration data.

Mode	m	n	$K_{mn}\ [m^{-2}]$	$f_n\ [Hz]$	$\omega_n\ [rad/s]$
1	1	1	0.0151	8.25	51.84
2	1	2	0.0234	13.85	87.02

- $\boldsymbol{E = 64.2\ GPa}$

4.3 Rayleigh Damping

To calculate the Rayleigh damping, values for the damping ratios corresponding to certain frequencies are required. These values are presented in Table 6.

Table 6: Damping ratios and respective frequencies.

$f\ [Hz]$	$\omega\ [rad/s]$	ξ [%]
8.25	51.84	2.391
9.00	56.55	0.579
13.85	87.02	0.976

The frequency from the second row is similar to the frequency from the first row, but their corresponding damping ratios are very different, which reveals a lack of precision of the measured damping ratios. This also indicates that the damping ratios corresponding to the frequencies contained within $[8.25, 9]\ Hz$ probably range from $\xi = 0.579$ % to $\xi = 2.391$ %. As such, the following values are considered:

- $\omega = \frac{8.25+9}{2} = 8.625\ Hz$
- $\xi = \frac{2.391+0.579}{2} = 1.485$ %

This set of values is as good an estimate as other sets of values contained in the intervals mentioned above, seeing that determining their accuracy is impossible. The coefficients required to estimate the Rayleigh damping matrix are determined by introducing these values into (3.10).

5. RESULTS

Several classes of vehicles can cross a bridge, including: motorcycles, cars, vans, single unit trucks and buses, and single and multi-trailer trucks. Information withdrawn from a passage log created on May 10th, from 10:40 AM to 1:10 PM, can be observed in Table 7. A passage log is a document where the time a vehicle starts crossing the bridge is registered, as well as the time it takes to cross the bridge. Table 5 also contains estimates for the weight of each type of vehicle.

In addition to the vehicle's weight, its number of axles and the distance between each axle are also required to estimate the acceleration and deformation signals that they produce. Estimates for these variables are presented in Table 8 for the relevant vehicle types. Small motorcycles and cars are considered irrelevant, due to their small weight and percentage of passages.

Table 7: Number of passages and estimates for the weight.

Type of vehicle	Number of passages (N_p)	$m\ [kg]$
Small motorcycle	1 (1%)	250
Small car	1 (1%)	950
Medium car	45 (51%)	1650
Large car	4 (5%)	2350
Pickup	6 (7%)	2700
Light van	27 (31%)	2700
Heavy van	2 (2%)	6350
Single unit truck/bus	1 (1%)	9075
Single unit truck/bus	1 (1%)	11800

Table 8: Number of axles and distance between axles.

Type of vehicle	Number of axles	$d_{1-2}\ [m]$	$d_{2-3}\ [m]$
Medium car	2	2.65	—
Large car	2	3.04	—
Pickup	2	3.20	—
Light van	2	3.10	—
Heavy van	2	3.51	—
Single unit truck/bus	2	5.27	—
Single unit truck/bus	3	5.97	1.47

Distances d_{1-2} and d_{2-3} represent the distance between the first and second axle, and the distance between the second and third axle, respectively.

5.1 Relevant Signals for the Case Study

The relevant signals for the case study are the ones produced by the relevant vehicle types travelling at their respective average velocities. These velocities are presented in Table 9.

Table 9: Average velocity for each vehicle type.

Type of vehicle	Average velocity [km/h]
Medium car	32.48
Large car	38.15
Pickup	34.25
Light van	40.66
Heavy van	27.85
Single unit truck/bus	29.32

To estimate the signals produced by a vehicle, the weight supported by each axle is required. These weights can be obtained by applying the static equilibrium equations. In its turn, these equations are solved using the values from Table 5 and Table 6 and the assumption that a vehicle's center of mass is equidistant from its front and rear axles. The signals produced by a single unit truck/bus with three axles travelling at its average velocity is shown in Figure 7.

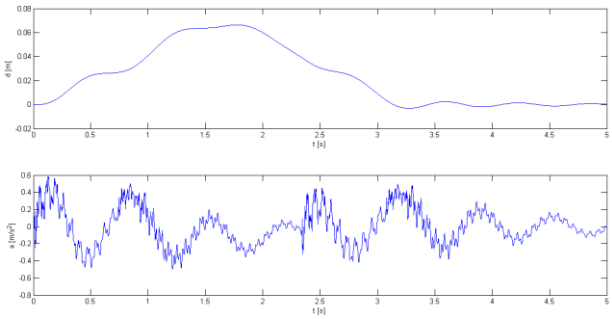

Figure 7: Signals produced by a three-axle bus.

The deformation (in terms of strain) is given by [5]:

$$\varepsilon_x(x,y,t) = -y\frac{\partial^2 w(x,t)}{\partial x^2} \qquad (18)$$

where $w(x,t)$ is the vertical displacement of the beam at position x and instant t, and y is the distance from the neutral axis.

This strain signal can be observed in Figure 8.

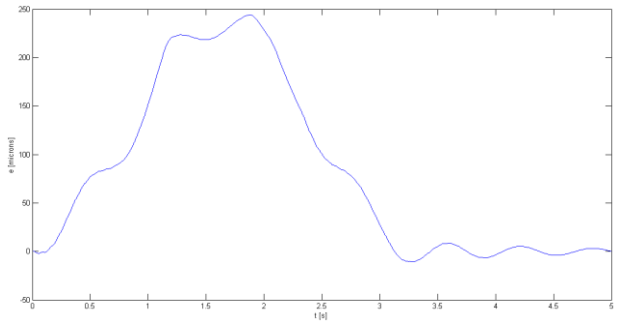

Figure 8: Computational strain signal.

5.2 Comparison Between Computational and Real Signals

According to the passage log, a three-axle bus crossed the bridge at May 10th, 2018, 10:40 AM. In its turn, the data collected by the accelerometers and extensometers from January 1st to January 10th confirms that a certain vehicle crosses the bridge every three days at approximately 10:40 AM. As such, to validate the computational model, the real signals measured at 10:40 AM (every three days) must be compared to the computational signals estimated for a three-axle bus. During the ten days when the data was collected, the three-axle bus crossed the bridge at January 3rd, January 6th and January 9th. The deformation signals measured at January 3rd by the relevant extensometers can be observed in Figure 9 and Figure 10.

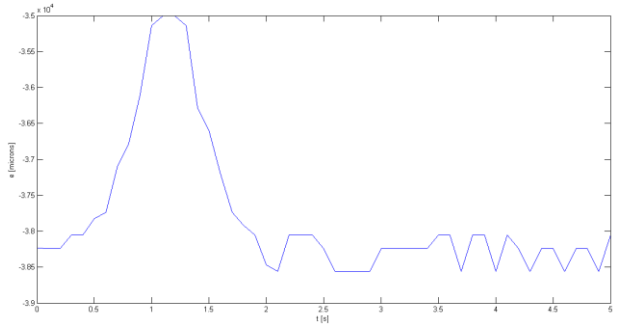

Figure 9: Real strain signal (1).

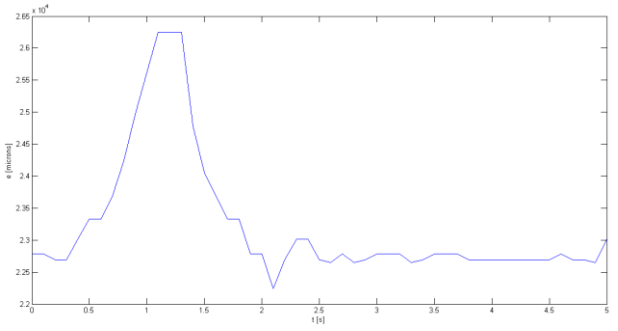

Figure 10: Real strain signal (2).

Although the shape of the computational signal is similar to the shape of the signals measured with the relevant extensometers, their amplitudes are very different.

5.3 Bending Stiffness

If the case study structure is to be treated as a beam, its properties and/or geometry need to change, so that the real signals measured by the relevant extensometers fit their computational signal as best as possible. This fluctuation of properties and geometry can be performed by varying the bridge's flexural rigidity or bending stiffness (EI).

The initial value for the bending stiffness is obtained from the second moment of inertia and Young's modulus determined in the case study section:

- $E = 64.2\ GPa$
- $I = 3.38 \cdot 10^{-3}\ m^4$
- $EI = E \cdot I = 0.217\ GPa \cdot m^4$

Figure 11 shows the computational signals varying with the bending stiffness, as well as the respective real signals.

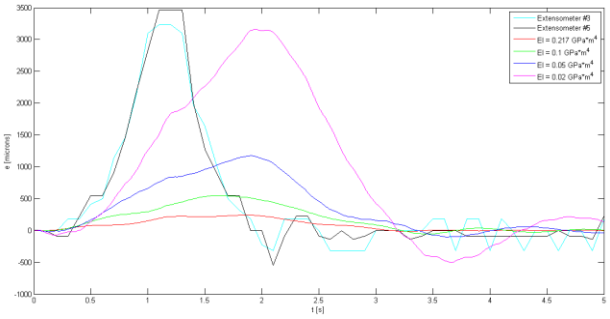

Figure 11: Real signals and computational signals.

The smaller the bending stiffness is, the more accurate the computational signal is, until its amplitude reaches the same amplitude of the real signals. After that, decreasing the bending stiffness also decreases the accuracy. Also, fluctuating one variable is usually not enough to fit computational signals with the real signals, as it can be observed by the increase of the offset time with the amplitude. To adjust this time offset, other properties and geometries, such as the density and the cross-sectional area, respectively, have to be considered. While the computational model returns very inaccurate results for the properties and geometries calculated in section 4, it can be applied with a reasonable accuracy if these values are

optimized. In other words, this model appears to be valid, and its accuracy is heavily dependent on the optimization of its inputs.

6. CONCLUSIONS AND FURTHER RESEARCH

This final section presents the main conclusions withdrawn from the paper, as well as its limitations and respective refinements implementable in future work.

6.1 Further Research

The computational model appears to be valid for the case study bridge structure and, therefore, it might be useful for other bridge structures with similar characteristics. However, its accuracy depends heavily on an optimization fit which may not always be as easy to perform as in this thesis, depending on such factors as the available data and complexity of the structure, among others.

Also, an SFSF plate (a rectangular plate that is simply supported on two opposite edges and free on the remaining edges) appears to be a good approximation for the case study structure, and in its turn a SSSS plate (rectangular plate simply supported on all edges) is a good approximation for a SFSF plate. However, a beam structure is an oversimplification for the case study bridge, if its properties and geometries are not optimized.

6.2 Limitations

The greatest limitation of the present work is the oversimplification of the beam structure to analyze bridge structures, which contain a higher complexity than a beam. Moreover, a major limitation consists of the lack of data about the traffic in the case study bridge, which is very important not only to estimate the computational signals during a certain period of time, but also to compare them to the corresponding real signals. In its turn, this comparison is essential to optimize the properties of a bridge structure defined as a beam.

Other limitations include the lack of vibration data, in terms of natural frequency and damping ratio, as well as its low precision. These limitations made it very difficult to estimate an accurate global damping matrix, as evidenced by the time offset between the real signals and the computational signals, despite their similarity in terms of shape.

Finally, the uncertainty of the loading and resistance data, namely the vehicle's characteristics and the bridge's properties and geometries, respectively, also constitute relevant limitations of the present work.

6.3 Future Work

Since a beam is a very simple structure, either its properties and geometries are optimized, or a more complex structure needs to be considered.

Fully optimizing the characteristics of a bridge defined as a beam requires a significant amount of data about its usual traffic, as well as sensors that measure important variables, including accelerations and deformations, at strategic points. The quantity of sensors and their position depend on the complexity and size of the bridge. Obtaining this information is usually very difficult and, consequently, a full optimization procedure would be hard to obtain under such circumstances. Nevertheless, a computational optimization procedure should be developed to find the physical parameters by fitting the measured signals to the computational signals, allowing variations in the bending stiffness as well as damping constants.

If the necessary time, resources and data to analyze a 3D structure are available, the bridge structure can be defined as a thick plate, for example. Otherwise, 2D structures may also be used, such as thin or moderately thick plates.

As for the global damping matrix, it requires more vibration data and a greater precision of this data to be estimated with a higher accuracy. A larger amount of vibration data allows the application of more flexible Rayleigh damping models, such as the damping models described in subsection 3.2.2, as well as a more accurate application of the normal Rayleigh damping model described in subsection 3.2.1. This data also needs to be more precise, since the expanded damping models are more sensitive to the natural frequencies and corresponding damping ratios than the normal damping model.

Furthermore, the uncertainty of the loading data given by the vehicles' characteristics can be reduced by creating more frequent passage logs. These logs contain accurate information about passing vehicles, as well as the time they start crossing the bridge. Therefore, the acceleration and deformation signals measured by the movement sensors at a certain time can be associated to the corresponding vehicle.

7. REFERENCES

[1] Google, [Online]. Available: https://maps.google.com/.

[2] NTSB, "Collapse of Pedestrian Bridge Under Construction," Miami, Florida, 2018.

[3] VESAM, "Ponte das Várzeas".

[4] "Revolvy," [Online]. Available: https://www.revolvy.com/page/List-of-bridge-failures.

[5] A. Araújo and N. Silvestre, "Elementos Bidimensionais," in Mecânica Estrutural, 2014, pp. 205-325.

[6] A. Araújo and N. Silvestre, "Sistemas Contínuos Unidimensionais," in Mecânica Estrutural, 2014, pp. 99-204.

[7] K.-J. Bathe, Finite Element Procedures, Englewood Cliffs, N. J.: Prentice Hall, 1996.

[8] F. P. Beer, E. R. Johnston, J. T. DeWolf and D. F. Mazurek, Mechanics of Materials, 5th ed., Global Edition, 2012.

[9] V. N. V. Do, T. H. Ong and C. H. Thai, "Dynamic responses of Euler-Bernoulli beam subjected to moving vehicles using isogeometric approach," Applied Mathematical Modelling, vol. 51, pp. 405-428, 2017.

[10] N. E. Dowling, Mechanical Behavior of Materials, 4th ed., Pearson Education, 2012.

[11] M. K. Lee, M. H. Fouladi and S. N. Namasivayam, "Natural frequencies of thin rectangular plates using homotopy-perturbation method," Applied Mathematical Modelling, vol. 50, pp. 524-543, 2017.

[12] M. Liu and D. G. Gorman, "Formulation of Rayleigh damping and its extensions," Computers & Structures, vol. 57, no. 2, pp. 277-285, 1995.

[13] E. Pollock. [Online]. Available: https://www.engineering.com/BIM/ArticleID/17517/Italys-Morandi-Bridge-CollapseWhat-Do-We-Know.aspx.

[14] J. N. Reddy, An Introduction to the Finite Element Method, McGraw Hill Higher Education, 1994.